Boundary-layer seeing measurements in the Canadian High Arctic

Paul Hickson*[a], Ray Carlberg[b], Ronald Gagne[a], Thomas Pfrommer[a], René Racine[c], Matthias Schöck[d,e], Eric Steinbring[e], Tony Travouillon[d]

[a]Dept. of Physics & Astronomy, Univ. of British Columbia, 6224 Agricultural Rd., Vancouver, BC V6T 1Z1, Canada; [b]Dept. of Astronomy & Astrophysics, Univ. of Toronto, 50 St. George St., Toronto, ON M5S 3H4, Canada; [c]Université de Montréal, Département de physique, CP6128, succ. centre-ville, Montreal, QC H3C 3J7, Canada; [d]Thirty Meter Telescope, California Institute of Technology, 1200 E. California Blvd., Pasadena, CA 91125; [e]NRC Herzberg Institute of Astrophysics, 5071 W. Saanich Rd., Victoria, BC V9E 2E7, Canada;.

ABSTRACT

As part of a program to measure and evaluate atmospheric turbulence on mountains at the most northerly tip of North America, we have deployed two SODARs and a lunar scintillometer at the Polar Environment Atmospheric Research Lab (PEARL) located on a 600m-high ridge near Eureka on Ellesmere Island, at 80° latitude. This paper discusses the program and presents a summary of ground-layer turbulence and seeing measurements from the 2009-10 observing season.

Keywords: site characterization, optical turbulence, boundary layer, seeing, arctic

1. INTRODUCTION

The Earth's polar regions offer significant advantages for ground-based optical and infrared astronomy. These include cold, dry conditions, long periods of darkness, and the potential for unsurpassed seeing. Observations from the Antarctic glacial plateau[1-7] indicate that above a strong boundary layer at the ice surface there is relatively little high-altitude turbulence. Using a combination of MASS and SODAR data, Lawrence et al.[5] estimated that the free atmosphere (i.e. above the boundary layer) at Dome C contributes a median seeing of 0.27 arcsec. It was later established that as the winter progresses, strong turbulence develops within the lower 0.2 km of the atmosphere above Dome C. This surface layer results in poor seeing conditions at the surface[6,7]. Balloon-born microthermal sensors provide a direct means to probe the turbulence profile in the atmosphere, and data from a series of 19 balloons launched at Dome C indicates a free atmosphere contribution of approximately 0.25 arcsec above the surface layer, at an altitude of 200 m[7]. This value is considerably lower than the free-atmosphere turbulence contribution (~0.33 arcsec) measured for the best mid-latitude sites, such as Mauna Kea[8].

The excellent free atmosphere seeing measured above the Antarctic ice cap arises from stable winter atmospheric conditions in the polar region. The inner edge of the Antarctic polar vortex marks a boundary between strong high-altitude global circulation and a central region of low-vorticity that typically extends to the outer part of the Antarctic continent. Within this region, wind speeds are lower and the shear zones found in association with mid-latitude jet streams are absent. However, the persistence of a strong boundary layer over the Antarctic ice plateau complicates the exploitation of the excellent free-atmosphere seeing[7].

The exciting results from Antarctica have motivated our team to look towards the opposite pole of the Earth. The Arctic also develops a strong winter polar vortex, within which stable conditions are expected. The inner boundary of the vortex is found typically at latitudes of 60° - 70°. The Canadian Arctic archipelago extends to 83°, usually inside the polar vortex. Moreover, this is a mountainous region which has the advantages of local topographical relief and a rocky surface common to established telescope sites. Many high, isolated peaks are near the seacoast, avoiding the conditions responsible for the strong surface-layer turbulence blanketing the central Antarctic icecap. An additional advantage of the High Arctic is accessibility. Major permanent bases (Alert at 82° and Eureka at 80°) are accessible by air year-round. Both are military outposts with manned weather stations served from southern Canada by large cargo planes. Eureka is supplied annually by ship.

*hickson@physics.ubc.ca; phone 1 604 822-3853; fax 1 604 822-5324

Ground-based and Airborne Telescopes III, edited by Larry M. Stepp, Roberto Gilmozzi, Helen J. Hall
Proc. of SPIE Vol. 7733, 77331R · © 2010 SPIE · CCC code: 0277-786X/10/$18 · doi: 10.1117/12.857409

Three years ago, our team began a program of in-situ testing of mountain sites in Northern Ellesmere Island. Stations were deployed by helicopter, during summer, at three locations near the northwestern coast, to measure weather and sky conditions throughout the year. The results of this work are described elsewhere[9]. They indicate that during the winter months, mountains in the region have high clear-sky fractions, and experience low wind speeds. However, it has not yet been possible to measure the seeing because of the limited access to these remote high-altitude locations.

In 2009, we began an investigation of a more-accessible site near Eureka with the specific aim of characterizing the ground-layer seeing. On a 600m-high ridge 15 km from the main base, a consortium of Canadian universities and government agencies operates the Polar Environment Atmospheric Research Laboratory (PEARL) - the most northerly permanent manned research station in the world[10]. In the summer of 2009, we deployed two SODARs and a lunar scintillometer, the Arctic Turbulence Profiler (ATP) designed to measure ground-layer turbulence. Details of our program and the scientific results will be presented in a separate paper. Here, we present a brief overview and summarize some initial results from the ATP instrument.

2. THE SITE

The PEARL location and building is shown in Figs. 1 and 2. The laboratory is located at 80.05352°N, 86.41652°W, atop a ridge extending along a north-south line. A parallel ridge lies approximately 0.5 km to the west. Beyond that the terrain falls sharply to the south and west, and more gradually to the north and east. Fjords lie to the west and north, with higher (~2000 m) mountains beyond. The altitude of the site is 615 m MSL, although the cold winter temperatures result in a typical pressure altitude of about 730 m.

Climate records, spanning 50 years, are available from the Environment Canada weather station at Eureka[11]. In mid-winter, the temperature at Eureka typically falls to -38° C, although temperatures as low as -55° C have been recorded. For the 6 month period of October - March, the mean temperature is -33.4° C.

During the winter months, the prevailing wind direction at Eureka is from the east with an average speed of 2.2 m/s. However, wind speeds exceeding 40 m/s can occur during winter storms. Wind speeds exceeding 14.4 m/s and 17.5 m/s occur on average 1.8 and 0.7 days per month, respectively.

The PEARL building is designed for the deployment of atmospheric instrumentation. It has a flat roof accessible by an external stairway, with power and communications ports insulated from the heated laboratory space below. Power is supplied from Eureka. A satellite link provides a connection to the internet, allowing instruments at PEARL to be accessed and controlled remotely. A road leads to the site, providing vehicle access in all but the worst weather.

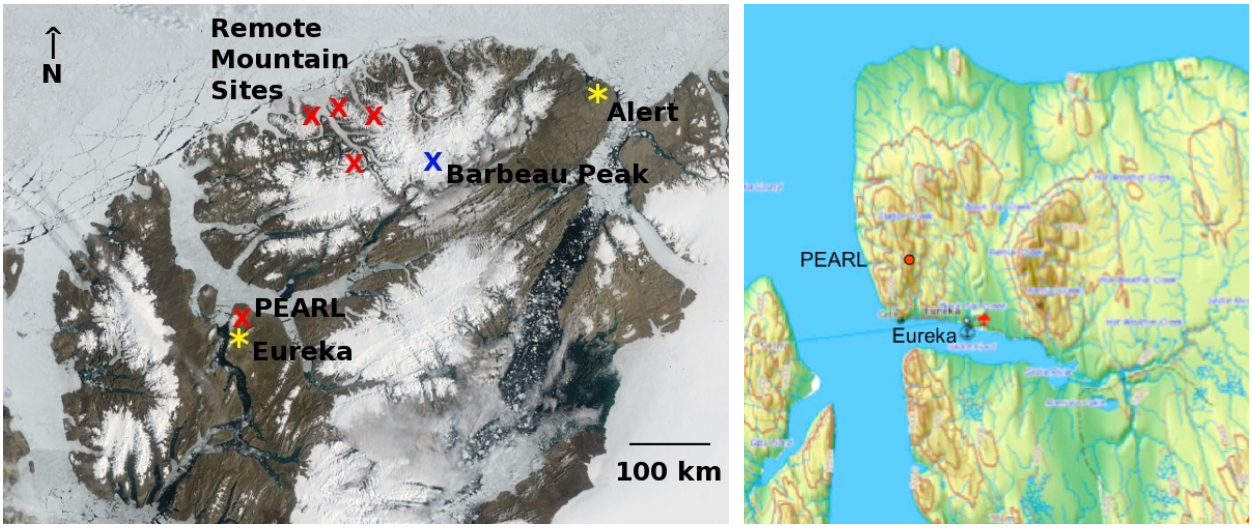

Figure 1. Northern Ellesmere Island (left panel), showing the location of the PEARL research station and the high, remote mountain sites being investigated by our team. Barbeau Peak is the highest mountain on Ellesmere Island, reaching an elevation of 2616 meters. The right panel gives an expanded topographical view of the PEARL region.

3. THE INSTRUMENT

The ATP is a lunar scintillometer (SHABAR) modeled after a similar instrument installed and operated at Cerro Tololo (Chile) by the University of British Columbia (UBC), which we shall call the Chilean Turbulence Profiler (CTP)[12]. The ATP was designed by Pfrommer and Hickson and built by the UBC Physics and Astronomy department machine and electronic shops over an 18-month period. It employs 48 photodiode sensors, arranged in 6 rings, each having 8 diodes, positioned along a vertical axis. Each diode has an unvignetted field of view approximately 36° horizontally by 22° vertically. At any given time, the Moon is visible to one photodiode in each of the six rings. As the Earth rotates, the Moon illuminates successive photodiodes, moving from one to the next in 2.4 hours (the two northermost positions do not have sensors, but the Moon is rarely high enough to observe in that direction). In this way, the instrument can follow the moon continuously during the night, without requiring any mechanical tracking. In fact the ATP has no moving parts whatsoever. The instrument is modular, designed to be transportable in sections by helicopeter, for future deployment at remote sites. Optical windows protect and seal the detector assemblies. There are no lenses or mirrors, but a single optical filter is located in front of each photodiode. Ellesmere Island is close to the center of the auroral circle, so auroral sky emission is not expected to be significant for astronomical observations. However, the Moon is never far above the horizon, and each diode views a large area of sky, so we included a filter as a precaution. The filter blocks all radiation having wavelengths less than 700 nm, which covers all of the most promenant auroral lines.

The current produced by each photodiode is amplified by a low-noise FET operational amplifier employing a 100 MOhm feedback resistor. Within each ring, the output of the amplifier connected to the illuminated photodiode is selected by an analog multiplexer, and then split into two channels: a DC-coupled low-gain channel and an AC-coupled high-gain channel. The AC channel employs a 5-pole analog Bessel filter that limits the bandwidth to 0.05 - 122 Hz (3 dB points). The output of either channel is selected by a multiplexer and digitized at 800 samples per second with 16-bit resolution. Amplifiers connected to non-illuminated photodiodes are powered off.

Every 120 seconds, 8000 samples of DC data are recorded, followed by 88000 samples of AC data. These data are recorded on solid-state flash memory. The instrument is controlled by a TS-7600 single-board computer running the TS-linux operating system. Communications with the outside world occurs via a 10/100 MBps ethernet interface. A control program, started automatically, keeps track of the positions of the Moon and Sun, and starts recording data from the appropriate photodiodes when the Moon is more than 19° above the horizon and the Sun is more than 9° below it.

Figure 2. The Polar Environment Atmospheric Research Laboratory (PEARL, left panel), as seen from the south, and the Arctic Turbulence Profiler (ATP) installed on the northwest corner of the roof (right panel).

Each window is coated with a conductive film, to which wires are bonded. Current is directed through the film by multiplexers, under program control. The purpose of this system is to keep the windows free of frost and ice. However, it did not perform as well as expected, and intervention was often needed by a PEARL technician to remove ice from the

instrument and windows. This was done by means of careful brushing with a broom and by the application of methanol. We suspect that the problem may arise from poor electrical conduction in the wire bonds and are investigating possible solutions.

During this testing phase, prior to deployment to a remote mountain site, the ATP was installed on the northwest corner of the roof of the PEARL building, as shown in Figure 2, approximately 6m above ground level.

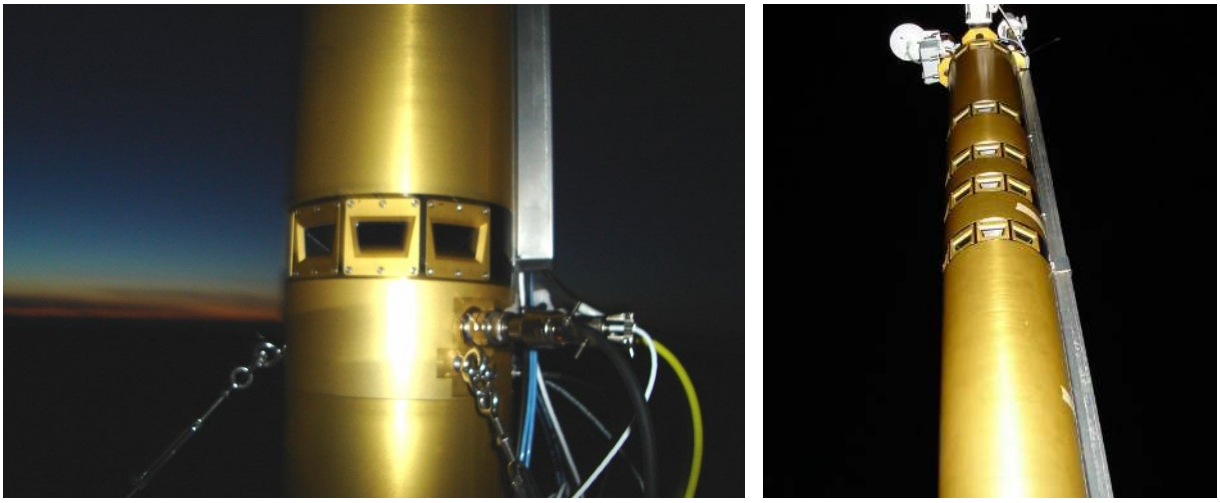

Figure 3. Night-time view of the lower (left) and upper (right) portions of the ATP. The individual windows covering each photodiode and the ring geometry can be seen. The metal channel on the north side of the instrument protects cables that run to environment sensors mounted on the top of the instrument.

4. DATA ANALYSIS

The lunar scintillometer provides a direct measurement of the turbulence (C_N^2) profile along the line of sight from the instrument to the Moon. The useful range of the instrument depends on the maximum separation between photodiodes, the lunar phase, and the outer scale of turbulence, and is typically ~1000 m for the ATP. For a lunar altitude of 30°, this corresponds to a height of ~500 m above the instrument. The height above ground of course depends on the local topography in the direction of the Moon.

The method of analysis follows that employed for the CTP[12]. Here we provide only a very brief overview, and highlight unique aspects of the ATP and differences from previous work. The fundamental equation connecting the data with the turbulence profile is

$$B_I(\mathbf{r}) = \int_0^\infty C_N^2(z\sin\zeta)\, W(\mathbf{r},z)\, dz, \tag{1}$$

which can be recognized as a Fredholm integral equation for the index-of-refraction structure constant, $C_N^2(h)$, assumed to be a function only of the height h above the instrument. Here $B_I(\mathbf{r})$ is the covariance of irradiance fluctuations measured by two photodiodes whose separation vector, perpendicular to the line of sight to the Moon, is $\mathbf{r}$. (Note that a vector is needed here, as the orientation of the baseline $\mathbf{r}$ with respect to the lunar terminator is important.) The quantity $W(\mathbf{r},z)$, called the weight function, describes the irradiance correlation produced by a unit impulse of turbulence located at range z. This function is computed using the well-established linear theory of the propagation of light through a randomly-varying medium having a von Karman turbulence spectrum. We compute weight functions numerically, including effects of lunar phase, illumination and orientation, detector geometry, diffraction and outer scale. A total of 453 weight functions were computed, one for every degree of lunar phase up to 150°, for three values of the outer scale. Following a review of published measurements, we selected an outer scale of 20 m for the ATP analysis. A representative set of response functions is shown in Figure 4.

The intensity distribution over the lunar disk was modeled by the Lommel-Seeliger law, which has its basis in the theory of radiative transfer of singly-scattered photons within the lunar regolith. Cast in terms of latitude θ and longitude ϕ, measured from the sub-Earth point on the lunar surface, the Lommel-Seeliger relation predicts an intensity

$$I(\phi,\alpha) = \frac{2I_0 f(\alpha)}{1 + \cos\phi / \cos(\phi - \alpha)}, \tag{2}$$

where α is the lunar phase angle (equal to zero at full moon). Note that the intensity is independent of latitude. Weight functions computed using this model were found to agree with those computed using CCD images of the moon to within ~10% for phases up to 150°.

The phase function $f(\alpha)$ does not enter into the weight function, as the latter depends only on dimensionless ratios. However it is useful in assessing the sky transparency. The empirical formula

$$f(\alpha) = 0.4\exp(-0.09\alpha) + 0.6\exp(-0.01\alpha), \tag{3}$$

where α is measured in degrees, agrees with the mean lunar flux at CTIO, measured by the CTP over a period of two years, to within 4% for lunar phases up to 150°.

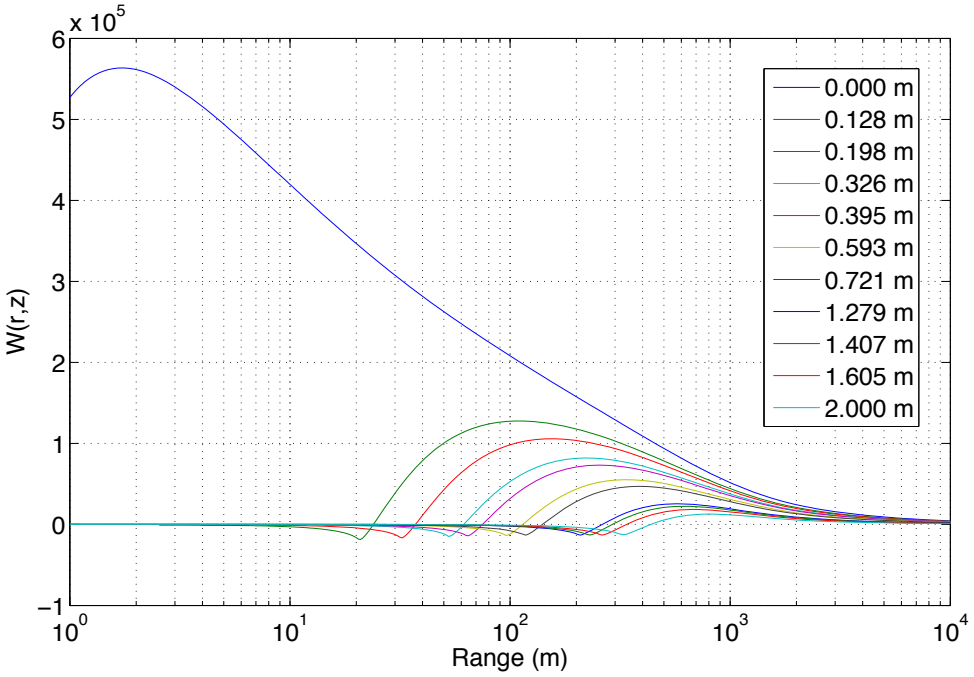

Figure 4. Response functions for the ATP baselines, computed for a lunar phase of 0° (full moon) and an outer turbulence scale of 20 m.

Equation (1) was solved by means of a Bayesian Markov chain Monte Carlo (MCMC) optimization. The model parameters were taken to be values of $\ln(C_N^2)$ at "pivot" heights of 0.1, 10, 20, 40, 80, 160, 320 and 640 m. The prior distribution of these quantities was taken to be log-normal, with a mean equal to the prediction of the Cerro Pachon turbulence model[13] and a standard deviation of 0.25[14]. Additional runs with prior parameters differing by as much as an order of magnitude were made which verified that the final results were not sensitive to the particular choice of values.

The likelihood function was computed from the difference between the measured covariances, and those computed by numerical integration of Equation 1. The values of $\ln(C_N^2)$ at heights other than the pivot values were determined by linear interpolation in log-log space (i.e. fit by a power law connecting the pivot points). Above the highest point, the

value of $\ln(C_N^2)$ was assumed to decrease as a power law to a height of 1280 m, above which the ground layer was assumed to make no significant contribution. Because the covariances on different baselines are intrinsically correlated, a covariance matrix was computed from the data, following the prescription of Tokovinin et al.[15] and its inverse employed in the computation of the likelihood.

For each 120 s data set, the 88,000 AC samples were normalized by dividing by the mean DC value of the corresponding photodiode (computed after an initial settling time). The covariance of these normalized intensities were computed for all 16 baselines (including the zero baseline, for which the median value of the variance was used). Data sets for which the weather was cloudy, or clearly non-photometric, were rejected.

A correction was made for diffuse light from the sky, which dilutes the observed lunar scintillation signal. The sky brightness is a function of angular distance from the moon, zenith angle and the lunar zenith angle and phase. The total contribution was determined by computing the sky brightness at intervals of 1 in angular distance, using the La Palma sky brightness calculator[16], and integrating the result over the photodiode field of view. The signal so obtained is comparable to observed values from photodiodes adjacent to the photodiode that was directly illuminated by the Moon. This resulted in a typical correction of ~3%.

A simple Metropolis-Hastings algorithm was found to be sufficient, and robust, for the MCMC optimization[17]. Convergence occurred rapidly, and always within the 3,000-iteration break-in period that was employed. Following the break-in period, 10,000 iterations were made to determine the posterior probability distribution of the model parameters, given the observational data.

Once the optimum turbulence model had been found, the seeing FWHM $\varepsilon(h)$, as a function of height h above ground, was obtained by integrating the model vertically upward, according to the relations for Kolmogorov turbulence,

$$\varepsilon(h) \simeq 0.976 \frac{\lambda}{r_0(h)}, \tag{4}$$

$$r_0(h) \simeq 0.185\, \lambda^{6/5} \left[\int_h^\infty C_N^2(x)\, dx \right]^{-3/5}. \tag{5}$$

These equations are appropriate for observations at the zenith using a small telescope. For apertures of several meters or more, the effect of a finite outer scale is to reduce $\varepsilon(h)$. The wavelength for all seeing calculations was taken to be 500 nm.

Since the ATP measures only ground-layer (GL) seeing (i.e. the contribution from the atmosphere below ~1 km), in order to estimate the total seeing, it is necessary to add a contribution from the free atmosphere (FA) according to

$$\varepsilon^{5/3} = \varepsilon_{GL}^{5/3} + \varepsilon_{FA}^{5/3}. \tag{6}$$

5. OBSERVATIONS AND RESULTS

The ATP was deployed at PEARL in late September, 2009, and we awaited the winter. Because of the high latitude, observations can only take place for a few days each month, when the moon is above the 19° altitude limit. The first data were obtained on November 4. Clouds, and problems with the sequencing of photodiodes (later corrected) limited the quantity of useful data. In all, a total of 388 minutes of photometric data were recorded during that lunar cycle.

On November 26, just days before the Moon was again within range, the instrument was badly damaged by a severe wind storm. The wind loading and vibration caused a 3/16" stainless steel cable, holding sections of the instrument together, to break. Although the optics and rings were not damaged, the interconnecting electrical cables were torn apart. The instrument was removed from the roof and the damaged components were identified by the PEARL technical staff. These were carried south on the next available charter flight, in December, and then shipped to UBC. There new parts were made, including new wiring harnesses and a stronger cable. These were sent to PEARL at the first opportunity, in January. The instrument was reassembled by the PEARL staff, and tested. Fortunately, everything worked. It was reinstalled on the roof in late January, in time for the coming February lunation. However, ice, frost and non-photometric conditions conspired to prevent us from obtaining any useful data that month.

We were finally able to obtain new data when the Moon once again climbed above the ATP altitude limit in late March. By this time, the Sun was above the horizon for almost half the day and barely reached our altitude (below the horizon)

threshold, so the available dark sky time was small. Nevertheless, we were able to obtain good data on four nights. For two days during this period (March 23 and 24), we observed relatively-strong ground-layer turbulence below 50 m. This occurred when the wind came from the northeast - probably the most unfavorable direction given the local topography (Figure 1).

Some representative results are shown in Figure 5. The figure shows the time history of the ground-layer seeing FWHM $\varepsilon(h)$ for four heights above ground. In all, 364 minutes of photometric data were obtained in March, giving a total of 752 minutes for the winter. Although the amount of data is limited, the data were obtained on 7 different days and over a range of seasons and wind conditions.

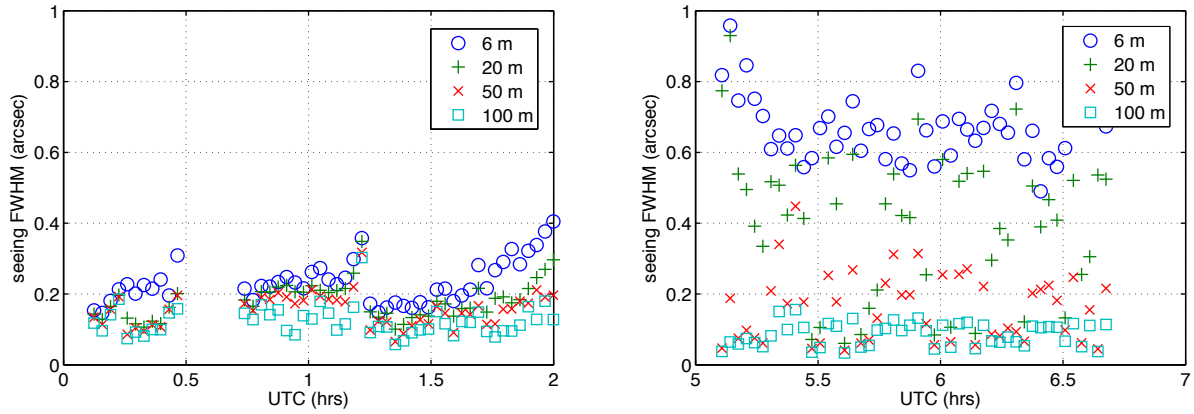

Figure 5. Ground-layer seeing derived from two sets of ATP data. The left panel, obtained on November 4, 2009., shows good seeing conditions. The right panel obtained on March 23, shows a period of poor seeing. The points indicate image FWHM predicted for a small telescope observing the zenith, at a wavelength of 500 nm, from the indicated height above ground, if there was no turbulence above ~1 km.

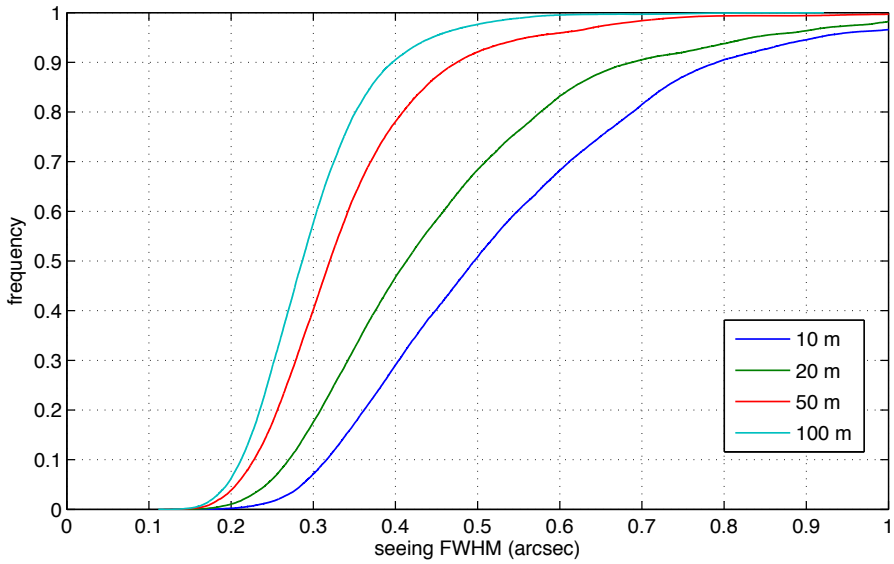

The cumulative frequency distribution of estimated total seeing, from all ATP data, is shown in Figure 6. The contribution from the free atmosphere was estimated by drawing samples randomly from a log-normal distribution having a standard deviation of 0.25 and a mean value corresponding to 0.25 arcsec. This value corresponds to the FA seeing determined from balloon measurements at Dome C, for a height above ground of 200 m.

Table 1 presents quartile values of seeing from the indicated height both for the ground layer alone and with an estimated 0.25 arcsec mean contribution from the free atmosphere. The results are based on all available ATP data, and random draws from a log-normal distribution for the free atmosphere component.

Table 1. Summary of seeing statistics.

	Ground-layer seeing (arcsec)			Estimated total seeing (arcsec)		
Height	25%	50%	75%	25%	50%	75%
10 m	0.246	0.390	0.564	0.383	0.496	0.649
20 m	0.178	0.274	0.427	0.325	0.413	0.591
50 m	0.093	0.158	0.220	0.268	0.320	0.388
100 m	0.068	0.106	0.146	0.244	0.287	0.337

6. DISCUSSION

The results presented in the previous section show that the ground layer at the PEARL site is often very weak. This is perhaps surprising given the relatively low altitude of PEARL compared to other sites. Can the results be believed? We think that they can, for a number of reasons. As Tokovinin et al. have emphasized [15], the lunar scintillometer is a relatively simple instrument, relying on well-established theory. The observed scintillation is weak, far from saturation, so linear propagation theory applies. Moreover, lunar scintillometers measure only a dimensionless quantity (the fluctuation in the logarithm of irradiance), so no calibration is required. Because the instrument gives a resolved turbulence profile, the effects of any local turbulence can be identified. This is not the case for instruments such as the differential image motion monitor (DIMM), which give only the turbulence integral, and can be biased by local turbulence [16].

As a test, the CTP scintillometer was operated simultaneously with Tokovinin's LuSci scintillometer[15] for several days in the spring of 2009. LuSci employs different optics, sensors, amplifiers and electronics and uses a different method of data analysis. Some results of this test are reported in these proceedings[18]. Despite the differences in the instruments and analysis, there is excellent agreement in the derived turbulence profiles and seeing values.

The ATP design differs somewhat from that of the CTP scintillometer. Apart from unimportant differences in mechanical design, the two instruments use different photodiodes, optics (the CTP has no blocking filter), preamplifiers and sampling rates. We therefore built a second set of ATP sensors and installed them along a beam attached to a tracking mount. This "portable" turbulence profiler (PTP) was sent to CFHT, to be used for turbulence measurements inside and outside the CFHT dome. One of us (Pfrommer) travelled to Hawaii to perform the measurements.

The PTP scintillometer was set up on the summit of Mauna Kea beside the tower that supports the CFHT MASS-DIMM monitor. Although the DIMM is at a height of ~6 m, and the PTP was at a height of ~ 1 m, the PTP turbulence profile can be integrated from a height of 6 m in order that the seeing measured by the two instruments may be compared. To predict the total seeing, the free-atmosphere seeing recorded by the MASS was added to the PTP ground-layer seeing, as per Equation (6). Nine hours of simultaneous data were acquired on the night of December 1, 2009. The results are shown in Figure 8. It can be seen that during the latter part of the night, the seeing derived from the PTP+MASS data and the DIMM seeing generally agree quite well. For the first three hours of the night, the PTP+MASS seeing was substantially higher than that obtained from the DIMM. This was due to high values of MASS seeing (often far exceeding the DIMM seeing). It is well known that in conditions of strong turbulence, the MASS overestimates the seeing. However, corrected data were not available at the time of writing. We conclude from this comparison that the PTP, and therefore the ATP, does accurately measure the ground-layer seeing.

The PTP scintillometer data from Mauna Kea provides an opportunity to directly compare the turbulence profiles above the CFHT summit area and PEARL. The PTP scintillometer was set up near the CFHT MASS-DIMM monitor tower,

approximately 50 m south of the CFHT dome, and in unobstructed air blowing from the east. Figure 8 shows the mean ground-layer seeing as a function of height for the two sites, as derived from nearly-identical instruments. The Mauna Kea results come from the ~8 hours of data obtained with the PTP on December 1, 2009 and the PEARL results come from ~5 hours of data obtained with the ATP on November 4, 2009 (the bulk of our 2009 data). It is evident that the turbulence profiles on these two nights are almost identical above a height of 20 m. Below this, a relatively strong ground layer is seen at Mauna Kea. In contrast, the ground-layer at PEARL was considerably weaker. Thus the seeing at PEARL, below a height of 20 m, was actually better than Mauna Kea (at least at this relatively-undisturbed location on the summit ridge).

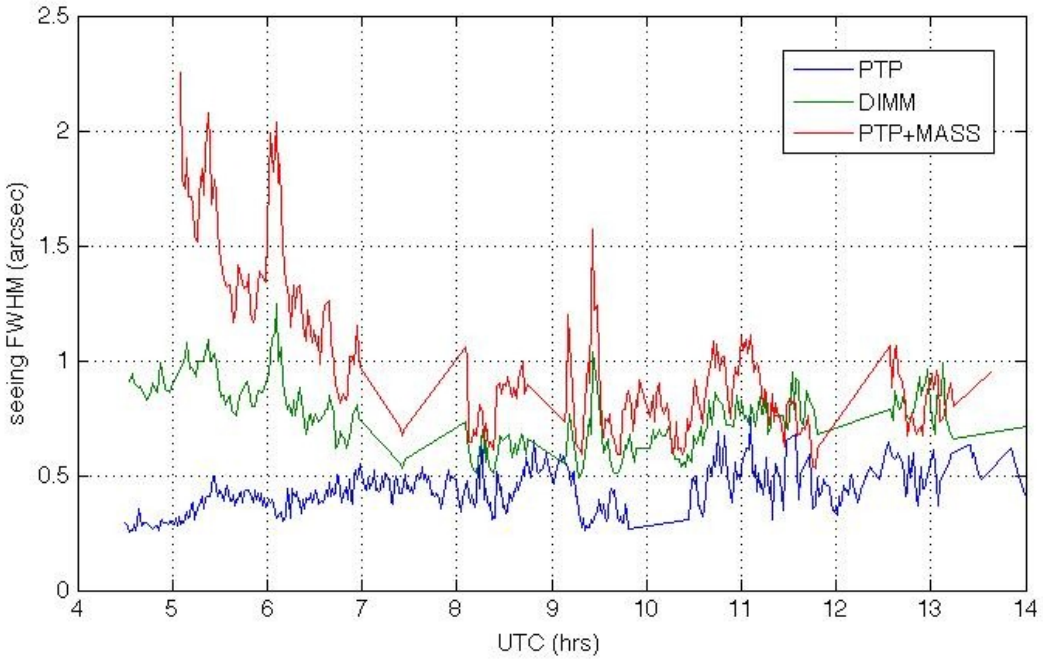

Figure 7. Results of simultaneous observations from the summit of Mauna Kea, by the PTP lunar scintillometer and the CFHT MASS-DIMM. The curves show (bottom to top) the ground-layer seeing above 6 m measured by the PTP scintillometer; The total seeing from a height of 6 m measured by the DIMM; the result of adding the high-altitude MASS seeing to the PTP ground-layer seeing (Equation 6). The high-altitude turbulence was unusually strong during the first half of this night, and it is known that the MASS overestimates the true seeing in such cases. This may account for the difference between the DIMM and PTP+MASS seeing estimates. (MASS and DIMM data were kindly made available by the Canada-France-Hawaii Telescope Corp.)

This surprising result is even more significant when one considers the free atmosphere. From the TMT site test campaign, Skidmore et al.[8] obtain a median value of 0.33 arcsec for the seeing in the free-atmosphere above Mauna Kea. This is considerably higher than the 0.25 arcsec found in Antarctica from balloon measurements at Dome C. If the free atmosphere in the High Arctic is comparable to that above Dome C, we must conclude that the total seeing at PEARL was in fact better that the seeing from the summit of Mauna Kea.

We plan to continue the ATP site testing at PEARL through the winter of 2010-2011. If all goes well this should greatly increase the size of our data set, and cover a wider range of environmental and atmospheric conditions. Our team is also planning to obtain simultaneous seeing observations for at least several winter nights by setting up and operating a DIMM on the roof of PEARL. The combination of DIMM and scintillometer data will allow the determination of the contribution of the free atmosphere to the seeing, and a test of the assumption that the free atmosphere in the High Arctic is similar to that at the opposite pole.

We are also continuing to collect data from the summit of Mauna Kea with the PTP scintillometer, in collaboration with CFHT. In addition to helping to characterize the airflow around the CFHT dome, these data will provide an important reference sample, from a site known to be outstanding, using the same instrumental technique as at PEARL.

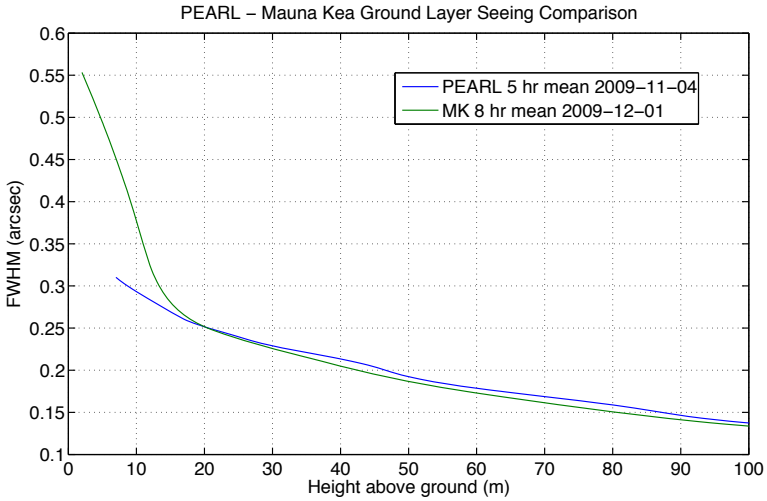

Figure 8. Mean ground-layer seeing as a function of height, obtained using similar lunar scintillometers at Mauna Kea and at PEARL. The data are from just one night, in each case, but were obtained during typical wind conditions at both sites.

It is important to emphasize that PEARL is an established research facility, containing instrument preparation rooms, a machine shop, and other infrastructure. Although it is situated atop a ridge, that location was not chosen with astronomical observations in mind. Our surprising initial results showing ground-layer seeing rivaling that of the best observing sites in the world, coupled with the expectation of weak high-altitude turbulence, warrants an expanded test program, both at PEARL and at other Ellesmere Island sites.

ACKNOWLEDGEMENTS

We are indebted to J. Drummond and the staff of PEARL who provided essential assistance with the installation, operation and repair of the ATP. Logistical support at Eureka was kindly provided by Environment Canada, as well as Natural Resources Canada through the Polar Continental Shelf Program. We also thank C. Veillet and the staff of the Canada-France-Hawaii Telescope, who provided an opportunity for us to make simultaneous observations with the PTP scintillometer and the CFHT MASS/DIMM. We thank A. Tokovinin for helpful discussions and for his collaboration with coordinated LuSci-CTP scintillometer measurements at CTIO. This work was supported by grants from the Natural Sciences and Engineering Research Council of Canada, the Canada Foundation for Innovation, the British Columbia Knowledge Development Fund, and by the National Research Council of Canada.

REFERENCES

[1] Marks, R. D., Vernin, J., Azouit, M., Briggs, J. W., Burton, M. G., Ashley, M. C. B., Manigault, J. F., "Antarctic site testing - microthermal measurements of surface-layer seeing at the South Pole," Astron. & Astrophys. Suppl. 118, 385-390 (1996).

[2] Marks, R. D., Vernin, J., Azouit, M., Manigault, J. F. and Clevelin, C., "Measurement of optical seeing on the high antarctic plateau," Astron. & Astrophys. Suppl. 134, 161-172 (1999).

[3] Marks, R. D., "Astronomical seeing from the summits of the Antarctic plateau," Astron. & Astrophys. 385, 328-336 (2002).

[4] Travouillon, T., Ashley, M. C. B., Burton, M. G., Storey, J. W. V., and Loewenstein, R. F., "Atmospheric turbulence at the South Pole and its implications for astronomy," Astron. & Astrophys. 400, 1163-1172 (2003).

[5] Lawrence, J. S., Ashley, M. C. B., Tokovinin, A. and Travouillon, T., "Exceptional astronomical seeing conditions above Dome C in Antarctica," Nature 431, 278-281 (2004).

[6] Aristidi, E., Agabi, A., Azouit, M., Fossat, E., Vernin, J., Sadibekova, T., Ziad, A., Martin, F., "Winter site testing at Dome C., Antarctica: first results," Bulletin de la Société Royale des Sciences de Liège 74, 5-6 (2005).
[7] Agabi, A., Aristidi, E., Azouit, M., Fossat, E., Martin, F., Sadibekova, T., Vernin, J., Ziad, A., "First whole atmosphere night-time seeing measurements at Dome C, Antarctica," Pub. Astron. Soc. Pacific 118, 344-348 (2006).
[8] Skidmore, W., Els, S., Travouillon, T., Riddle, R., Schöck, M., Bustos, E., Seguel, J., Walker, D., "Thirty Meter Telescope site testing V: seeing and isoplanatic angle," Publ. Astron. Soc. Pacific 121, 1151-1166 (2009).
[9] Steinbring, E., Leckie, B., Welle, P., Hardy, T., Cole, B., Bayne, D., Croll, B., Walker, D., E., Carlberg, R. G., Fahlman, G. G., Wallace, B., Hickson, P., "Inuksuit: robotic astronomical site-testing stations in the Canadian High Arctic," Proc. SPIE, 7012, .70121V-70121V-12 (2008).
[10] http://candac.ca/candac/Facilities/facility.php?type=PEARL
[11] http://climate.weatheroffice.gc.ca/
[12] Hickson, P., Pfrommer, T., Crotts, A., "Optical turbulence profiles at CTIO from a 12-element lunar scintillometer," in Optical Turbulence, Astronomy meets Meteorology, ed. E. Masciadri and M. Sarazin, ESO, Germany (2008).
[13] Tokovinin, A., Travouillon, T., "Model of optical turbulence profile at Cerro Pachón," Mon. Not. Roy. Astron. Soc. 365, 1235-1242 (2006).
[14] Racine, R., private communication (2010).
[15] Tokovinin, A., Bustos, E., Berdja, A., "Near-ground turbulence profiles from a lunar scintillometer," Mon. Not. Roy. Astron. Soc. 404, 1186-1196 (2010).
[16] http://catserver.ing.iac.es/signal/signalsky.php
[17] Gregory, P., [Baysian Logical Data Analysis for the Physical Sciences], Cambridge University Press, Cambridge, 1-468 (2005).
[18] Tokovinin, A., "Where is the surface-layer turbulence?," Proc. SPIE 7733, in press (2010).
[19] Rajagopal, J., Tokovinin, A., Bustos, E., Sebag, J., "LuSci: a lunar scintillometer to study ground layer turbulence," Proc. SPIE 7013, 70131P-70131P-9 (2008).